INTERNATIONAL JOURNAL FOR NUMERICAL METHODS IN FLUIDS, VOL. 22, 43–66 (1996)

MODEL VERIFICATION ON 3D TIDAL CURRENT ANALYSIS IN TOKYO BAY

TOSHIO KODAMA

Engineering Research Institute, Sato Kogyo Co., Ltd., Nihonbashi Honcho 4-12-20, Chuo-ku, Tokyo 103, Japan

SAM S. Y. WANG

Center for Computational Hydroscience and Engineering, The University of Mississippi, University, MS 38677, U.S.A.

AND

MUTSUTO KAWAHARA

Department of Civil Engineering, Chuo University, Kasuga 1-13-27, Bunkyo-ku, Tokyo 112, Japan

SUMMARY

The results of a research project to verify the newly improved multiple-level model for 3D tidal current analysis in Tokyo Bay are presented. The improved multiple-level model includes additional effects due to Coriolis force, river inflows and wind shear stresses. Furthermore, a new numerical treatment of the open boundary condition was applied which effectively eliminated the spurious reflective waves often generated by various numerical methods simulating free surface flows. The mean (time-averaged or residual) and tidal currents in Tokyo Bay were simulated as examples to demonstrate the validity and capability of the newly improved multiple-level model. A series of numerical experiments was conducted to carefully examine the tidal circulations affected by the forcing factors of Coriolis force, river inflows and wind shears, both individually and combined. The numerical results demonstrated that the effects of each forcing term are physically reasonable, with the wind shear effect being the most significant and the case including all forcing terms being in best overall agreement with the field data collected in Tokyo Bay by the Ministry of Transportation. This study has contributed not only to the verification of the newly improved multiple-level model but also to the enhancement of the accuracy of numerical simulations of three-dimensional flow in coastal waters by this model.

KEY WORDS: multiple-level model; finite element method; open boundary condition; tidal current analysis

1. INTRODUCTION

Prediction of the three-dimensional structure of tidal currents in coastal waters is an important subject in the field of environmental and hydraulic engineering, because it is capable of correctly determining the flow directions in the upper and lower layers of coastal flows and the residual currents in coastal regions. Such predictions determine the accuracy in simulating transport phenomena such as convection–diffusion of heat, pollutants, etc. It is generally believed that the residual current (or base flow or mean flow) is affected more significantly by Coriolis force, river inflow, wind shear stress and density stratification effects than by tides. In the recent past, most numerical models applied to study coastal transport phenomena were either 2D or 3D without considering the effects of Coriolis force, river inflows and/or wind shears. Therefore the present study is intended to make a major improvement in the field.

A test case which numerically expresses the mean and tidal current flow phenomena in Tokyo Bay, Japan is presented. In the open literature the publications on numerical simulations of 3D free surface

CCC 0271–2091/96/010043–24

Received September 1994
Revised May 1995

flows are too numerous to discuss.[1-8] They have had some success in predicting the three-dimensional flow field in Tokyo Bay, but none of the reported studies has investigated the effects of the aforementioned forcing functions on the mean flows in a tidal bay. This paper presents the results of such an investigation utilizing the improved multiple-level model originally reported by Kawahara *et al*[3].

The multiple-level model in this study was developed based on a finite element method and is general enough to include the effects of Coriolis force, river inflows and wind shear stresses. The non-reflective wave condition developed recently by the first author was applied at the open boundary.

The formulation of the newly improved multiple-level model and the open boundary treatment are described first, then the simulation of wind-induced flow in a rectangular basin using the present method is shown. As a practical application the results of mean flow (residual current of tidal circulation) and tidal current in Tokyo Bay are given. The results of a series of systematic numerical experiments indicate which of the forcing factors is most instrumental in producing accurate results of numerical simulation of the tidal and residual currents. Finally, the result of a validation test of the model for tidal flow simulation of Tokyo Bay based on the designed test case is reported.

2. MODIFIED MULTIPLE-LEVEL MODEL

2.1. Basic equations

The multiple-level model proposed by Kawahara *et al.*[3] is modified for this study. The basic equations of the multiple-level flow are

$$\frac{\partial u}{\partial t}+\frac{\partial}{\partial x}(uu)+\frac{\partial}{\partial y}(uv)+\frac{\partial}{\partial z}(uw)=fv-\frac{1}{\rho}\frac{\partial p}{\partial x}+\frac{1}{\rho}\left(\frac{\partial \tau_{xx}}{\partial x}+\frac{\partial \tau_{xy}}{\partial y}+\frac{\partial \tau_{xz}}{\partial z}\right), \tag{1}$$

$$\frac{\partial v}{\partial t}+\frac{\partial}{\partial x}(uv)+\frac{\partial}{\partial y}(vv)+\frac{\partial}{\partial z}(vw)=-fu-\frac{1}{\rho}\frac{\partial p}{\partial y}+\frac{1}{\rho}\left(\frac{\partial \tau_{yx}}{\partial x}+\frac{\partial \tau_{yy}}{\partial y}+\frac{\partial \tau_{yz}}{\partial z}\right), \tag{2}$$

$$\frac{\partial p}{\partial z}+\rho g=0, \tag{3}$$

$$\frac{\partial u}{\partial x}+\frac{\partial v}{\partial y}+\frac{\partial w}{\partial z}=0, \tag{4}$$

where x, y and z represent Cartesian co-ordinates positive eastwards, northwards and upwards respectively, t is the time, u, v and w denote velocity components for x, y and z respectively and p and f are the pressure and Coriolis parameter respectively. The approximation of hydrostatic pressure distribution is employed for the momentum equation of vertical direction. The density of water, ρ, is treated as a constant in the horizontal direction, postulating that water is incompressible. The turbulent shear stress is expressed by τ_{xx}, τ_{xy}, τ_{xz}, τ_{yy} and τ_{yz} and is assumed to be a function of velocity gradient. The multilevel system is introduced in the vertical water depth direction as shown in Figure 1. A representative level in the multilevel system is referred to as $L^{(k)}$, where $L^{(k)}$ denotes the negative value of z measured from the mean water elevation. The surface level is expressed by $L^{(1)}$ and the bottom level is $L^{(b)}$. Henceforth the indicial notation and the summation convention with repeated indices have been employed in order to simplify the expressions. The subscript $(\ )_{,i}$ indicates partial differentiation with respect to the ith co-ordinate. The symbols δ_{ij} and ε_{ij} are Kronecker's delta function and

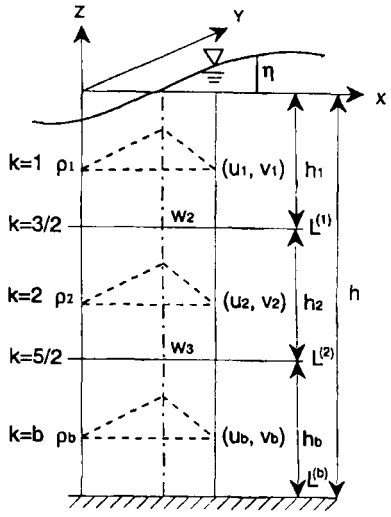

Figure 1. Level model

Edington's epsilon function respectively. Integrating the horizontal velocity over the (k)th water volume held between $L^{(k-1)}$ and $L^{(k)}$, the vertically averaged horizontal velocity is defined as

$$u_i^{(k)} = \frac{1}{h^{(k)}} \int_{L^{(k-1)}}^{L^{(k)}} u_i \, dz, \tag{5}$$

where the (k)th water volume thickness is expressed as

$$h^{(k)} = L^{(k)} - L^{(k-1)}. \tag{6}$$

The vertically averaged equations of momentum and continuity are defined from (1)–(4) using (5). The equation of momentum can be expressed as

$$\frac{\partial u_i^{(k)}}{\partial t} + u_j^{(k)} u_{i,j}^{(k)} + \frac{1}{h^{(k)}}[(u_i w)^{(k-1/2)} - (u_i w)^{(k+1/2)}] + \frac{1}{\rho^{(k)}} p_{,i}^{(k)} - f\varepsilon_{ij} u_j^{(k)}$$
$$= \frac{1}{\rho^{(k)} h^{(k)}}[h^{(k)} \tau_{ij,j}^{(k)} + (\tau_i^{(k)u} - \tau_i^{(k)l})], \tag{7}$$

where $\rho^{(k)}$ is the water density in the (k)th water volume, $p^{(k)}$ is the pressure computed by

$$p^{(k)} = \rho^{(1)} g\eta - \sum_{m=1}^{k-1} \rho^{(m)} g h^{(m)} - \rho^{(k)} g\left(z - \sum_{m=1}^{k-1} h^{(m)}\right), \tag{8}$$

with η the surface elevation measured from the mean water elevation, and the term $u_i w^{(k-1/2)}$ is given by

$$(u_i w)^{(k-1/2)} = w^{(k)} \tfrac{1}{2}(u_i^{(k)} + u_i^{(k-1)}),$$

with $w^{(k)}$ the vertical velocity component in the (k)th water volume.

The equation of continuity is written for the surface level as

$$\frac{\partial \eta}{\partial t} + \sum_{l=1}^{b} (h^{(l)} u_i^{(l)})_{,i} = 0. \tag{9}$$

The continuity equation for the middle layer is

$$w^{(k)} = -\sum_{l=k}^{b} (h^{(l)} u_i^{(l)})_{,i}. \tag{10}$$

The turbulent shear stress is assumed as

$$\tau_{ij}^{(k)} = A_l^{(k)} (u_{i,j}^{(k)} + u_{j,i}^{(k)}), \tag{11}$$

where A_l is the eddy viscosity coefficient. The interface shear stress is modelled using the quadratic friction law. For the surface level the wind friction is introduced in the form

$$\tau_i^{(1)u} = C^* \rho_a W W_i, \tag{12}$$

where C^*, ρ_a, W and W_i are the wind drag coefficient, air density, magnitude of wind velocity and wind velocity component respectively. For the intermediate level the following friction terms are used:

$$\tau_i^{(k)u} = \frac{f_m}{2h^{(k)}} (\rho^{(k-1)} + \rho^{(k)})(u_i^{(k-1)} - u_i^{(k)}) \Delta V^{(k)} \quad \text{(upper side)}, \tag{13}$$

$$\tau_i^{(k)l} = \frac{f_m}{2h^{(k)}} (\rho^{(k)} + \rho^{(k+1)})(u_i^{(k)} - u_i^{(k+1)}) \Delta V^{(k)} \quad \text{(lower side)}, \tag{14}$$

where f_m is the friction coefficient of the interface and

$$\Delta V^{(k)} = [(u_i^{(k-1)} - u_i^{(k)})(u_i^{(k-1)} - u_i^{(k)})]^{1/2}. \tag{15}$$

The bottom friction

$$\tau_i^{(b)l} = \frac{f_b}{h^{(b)}} \rho^{(b)} u_i^{(b)} (u_k^{(b)} u_k^{(b)})^{1/2} \tag{16}$$

is used, where f_b is the friction coefficient of the bottom.

The following two types of boundary condition are considered. On the land boundary Γ_L at the (k)th level the velocity is specified as

$$u_n^{(k)} = 0 \quad \text{on } \Gamma_L, \tag{17}$$

where n denotes the normal direction to the boundary. On the open boundary Γ_O the following boundary condition is imposed:

$$\bar{u}_n^{(k)} = \frac{g}{C} (\bar{\eta}^I n^+ + \bar{\eta}^R n^-) \quad \text{on } \Gamma_O, \tag{18}$$

where $C = \sqrt{(gh)}$ denotes the phase speed, I and R refer to the incident and reflective wave components respectively, the overbar indicates values on the open boundary and the symbols n^+ and n^- represent unit normal vectors in positive and negative directions to the boundary respectively.

The incident wave condition is given as the known function

$$\bar{\eta}^I = \sum_{m=1}^{N_c} a_m \sin(k_n^m n - \omega_m t - \kappa_m), \tag{19}$$

where a_m, k_n^m, ω_m and κ_m are the amplitude, wave number, angular frequency and phase delay respectively and N_c is the number of constituents. The reflective wave $\bar{\eta}^R$ is the unknown. The procedure whereby the reflective wave component is determined and the open boundary condition to be imposed are explained in the following subsection.

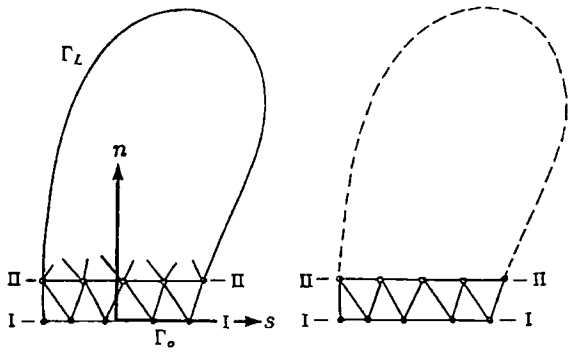

(a) Whole domain (b) Subdomain

Figure 2. Conceptual figures of finite element idealization

2.2. Open boundary condition

The computational procedure to treat the open boundary condition is given in this subsection. The conceptual figure of finite element discretization is shown in Figure 2(a). Along the open boundary the co-ordinate s is located and n is normal to this boundary. The line I–I ($n = n_0$) corresponds to the open boundary. The line II–II ($n = n_0 + \Delta n$) is placed on a single layer of finite elements inside the domain. Figure 2(b) shows the subdomain which is used to compute the reflective wave component on the open boundary I–I.

It is assumed that the incident wave condition, i.e. the water elevation, can be expressed as a linear combination of the incident and reflective wave components:

$$\bar{\eta}(n_0, s, t) = \bar{\eta}^{\mathrm{I}}(n_0, s, t) + \bar{\eta}^{\mathrm{R}}(n_0, s, t). \tag{20}$$

Secondly, the boundary condition has to be imposed as

$$\bar{u}_n^{(k)}(n_0, s, t) = \frac{g}{C}[\bar{\eta}^{\mathrm{I}}(n_0, s, t)n^+ + \bar{\eta}^{\mathrm{R}}(n_0, s, t)n^-] \tag{21}$$

The incident wave condition is assumed to be a known function expressed as

$$\bar{\eta}^{\mathrm{I}}(n_0, s, t) = a_{\mathrm{I}} \sin(k_0 n_0 - \omega t - \kappa). \tag{22}$$

It is required to determine the reflective wave component which is essentially unknown. The logic of this treatment is explained as follows. Firstly, the initial values of variables at all nodal points are set to be zero. Secondly, in the whole domain the variables at all nodal points are calculated using the incident wave condition given by (19) together with the boundary conditions. At that time, computed values include both incident and reflective components. In parallel, in the subdomain the incident wave component at one mesh size inside the open boundary, i.e. the line II–II, can be computed under the same incident wave condition. Here, on the outlet boundary the progressive wave condition is imposed. Then the reflective wave component on the line II–II can be calculated by taking the difference between the component obtained in the whole domain and the incident wave component obtained in the subdomain. Thirdly, since the reflective wave component can be obtained on the line II–II, the reflective component which will propagate towards the open boundary (the line I–I) can be computed using the subdomain again. The progressive wave condition is also applied to the outlet boundary. Finally, the open boundary condition which should be imposed at the next time iteration can be calculated by taking the sum of the incident and reflective components which have been obtained by

the above procedure. Thus the subdomain is introduced as a dummy to obtain the reflective wave component.

The algorithm for the computation of the open boundary condition is shown below.

Step 0. Set $u_i^{(k)}(n, s, t_0) = 0.0$ and $\eta(n, s, t_0) = 0.0$ for all nodal points.

Step 1. Compute $u_i^{(k)}(n, s, t + \Delta t)$ and $\eta(n, s, t + \Delta t)$ in the whole domain with the incident wave conditions, $\bar{\eta}^{\mathrm{I}}(n_0, s, t)$ and boundary condition

$$\bar{u}_n^{\mathrm{I}(k)}(n_0, s, t) = \frac{g}{C}\bar{\eta}^{\mathrm{I}}(n_0, s, t)n^+.$$

Step 2. Compute $u_n^{\mathrm{I}(k)}(n_0 + \Delta n, s, t + \Delta t)$ and $\eta^{\mathrm{I}}(n_0 + \Delta n, s, t + \Delta t)$ in the subdomain with the incident wave conditions, $\bar{\eta}^{I}(n_0, s, t)$ and boundary conditions

$$\bar{u}_n^{\mathrm{I}(k)}(n_0, s, t) = \frac{g}{C}\bar{\eta}^{\mathrm{I}}(n_0, s, t)n^+,$$

$$u_n^{\mathrm{I}(k)}(n_0 + \Delta n, s, t + \Delta t) = \frac{g}{C}\eta^{\mathrm{I}}(n_0 + \Delta n, s, t + \Delta t)n^+.$$

Step 3. Compute the reflective wave component

$$u_n^{\mathrm{R}(k)}(n_0 + \Delta n, s, t + \Delta t) = u_n^{(k)}(n_0 + \Delta n, s, t + \Delta t) - u_n^{\mathrm{I}(k)}(n_0 + \Delta n, s, t + \Delta t),$$

$$\eta^{\mathrm{R}}(n_0 + \Delta n, s, t + \Delta t) = \eta(n_0 + \Delta n, s, t + \Delta t) - \eta^{\mathrm{I}}(n_0 + \Delta n, s, t + \Delta t).$$

Step 4. Set $t = t + \Delta t$.

Step 5. Compute $u_n^{\mathrm{R}(k)}(n_0, s, t + \Delta t)$ and $\eta^{\mathrm{R}}(n_0, s, t + \Delta t)$ in the subdomain with the incident wave conditions, $\eta^{\mathrm{R}}(n_0 + \Delta n, s, t)$ and boundary conditions

$$u_n^{\mathrm{R}(k)}(n_0 + \Delta n, s, t) = \frac{g}{C}\eta^{\mathrm{R}}(n_0 + \Delta n, s, t)n^-,$$

$$\bar{u}_n^{\mathrm{R}(k)}(n_0, s, t + \Delta t) = \frac{g}{C}\bar{\eta}^{\mathrm{R}}(n_0, s, t + \Delta t)n^-.$$

Step 6. Compute the open boundary condition for the whole domain,

$$\bar{u}_n^{(k)}(n_0, s, t + \Delta t) = \frac{g}{C}\bar{\eta}^{\mathrm{I}}(n_0, s, t + \Delta t)n^+ + \frac{g}{C}\bar{\eta}^{\mathrm{R}}(n_0, s, t + \Delta t)n^-,$$

and the incident wave condition

$$\bar{\eta}(n_0, s, t + \Delta t) = \bar{\eta}^{\mathrm{I}}(n_0, s, t + \Delta t) + \bar{\eta}^{\mathrm{R}}(n_0, s, t + \Delta t).$$

Step 7. Repeat the computations starting from Step 1.

By applying this procedure, the spurious reflective wave is completely eliminated on the open boundary.

2.3. *Finite element method*

The conventional Galerkin method is employed for the finite element formulation. The horizontal velocity components and water elevation for the (k)th level are interpolated in each finite element:

$$u_i^{(k)} = \Phi_\alpha u_{\alpha i}^{(k)}, \qquad \eta = \Phi_\alpha \eta_\alpha, \tag{23}$$

where Φ_α denotes the interpolation function for velocity and water elevation and $u_{\alpha i}^{(k)}$ and η_α are the velocity and water elevation at the αth node of each finite element respectively. As interpolation function, a standard linear function based on the three-node triangular element is used in this paper. The Galerkin procedure leads to the following finite element equations for the (k)th level: for the momentum equation

$$M_{\alpha\beta}\dot{u}_{\beta i}^{(k)} + K_{\alpha\beta\gamma} u_{\beta j}^{(k)} u_{\gamma i}^{(k)} + f\varepsilon_{ij} M_{\alpha\beta} u_{\beta j}^{(k)} + N_{\alpha i\beta} p_\beta^{(k)} + \frac{A_i}{\rho^{(k)}} S_{\alpha i\beta j}^{(k)} - (T_{\alpha i}^{(k)\mathrm{u}} - T_{\alpha i}^{(k)\mathrm{l}}) - \Pi_{\alpha i}^{(k)} = 0, \tag{24}$$

for the continuity equation of the surface level

$$M_{\alpha\beta}\dot{\eta}_\beta + \sum_{q=1}^{b} (h^{(q)} N_{\alpha i\beta} u_{\beta i}^{(q)}) = 0 \tag{25}$$

and for the continuity equation of the intermediate level

$$M_{\alpha\beta} w_\beta^{(k)} = -\sum_{l=k}^{b} (h^{(l)} N_{\alpha i\beta} u_{\beta i}^{(l)}), \tag{26}$$

where

$$M_{\alpha\beta} = \int_V (\Phi_\alpha \Phi_\beta)\mathrm{d}V, \qquad K_{\alpha\beta\gamma j} = \int_V (\Phi_\alpha \Phi_\beta \Phi_{\gamma,j})\mathrm{d}V, \qquad N_{\alpha\beta i} = \int_V (\Phi_\alpha \Phi_{\beta,i})\mathrm{d}V,$$

$$S_{\alpha i\beta j} = \int_V (\Phi_{\alpha,i}\Phi_{\beta,j})\mathrm{d}V + \int_V (\Phi_{\alpha,k}\Phi_{\beta,k})\delta_{ij}\,\mathrm{d}V,$$

$$T_{\alpha i}^{(k)\mathrm{u}} = \int_V (\Phi_\alpha \tau_i^{(k)\mathrm{u}})\mathrm{d}V, \qquad T_{\alpha i}^{(k)\mathrm{l}} = \int_V (\Phi_\alpha \tau_i^{(k)\mathrm{l}})\mathrm{d}V,$$

$$\Pi_{\alpha i}^{(k)} = \int_V \{\Phi_\alpha [(u_i w)^{(k-1/2)} - (u_i w)^{(k+1/2)}]\}\mathrm{d}V.$$

To solve the above finite equations, a numerical integration scheme in time has to be introduced. The integration scheme employed in this paper is a two-step explicit scheme.[9] The open boundary condition described in the previous subsection is used at every time step to solve the above equations.

3. MODEL VERIFICATION; WIND-INDUCED FLOW

A number of studies that treat wind-induced flow have been reported.[10–13] Tsanis also reviewed recent studies of wind-induced currents in coastal waters by both theoretical and experimental approaches.[14] Koutitas and O'Connor examined the computer modelling of three-dimensional coastal flow by the simulation of wind-driven flow.[15] Pearce and Cooper presented a three-dimensional model with the vertical eddy viscosity varying over the depth.[16]

The numerical test of a steady wind-induced flow in a uniform rectangular channel was carried out similarly to the studies mentioned above. A channel with a constant depth of 10 m and a length of

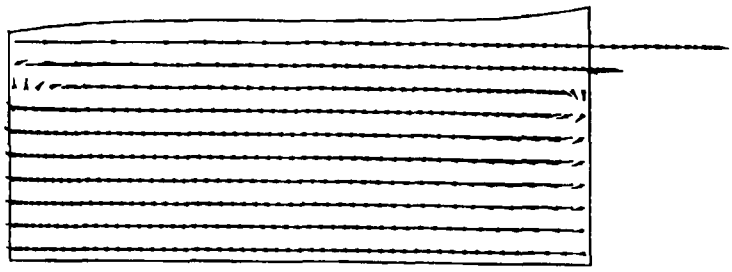

Figure 3. Computed velocity field of wind-induced flow

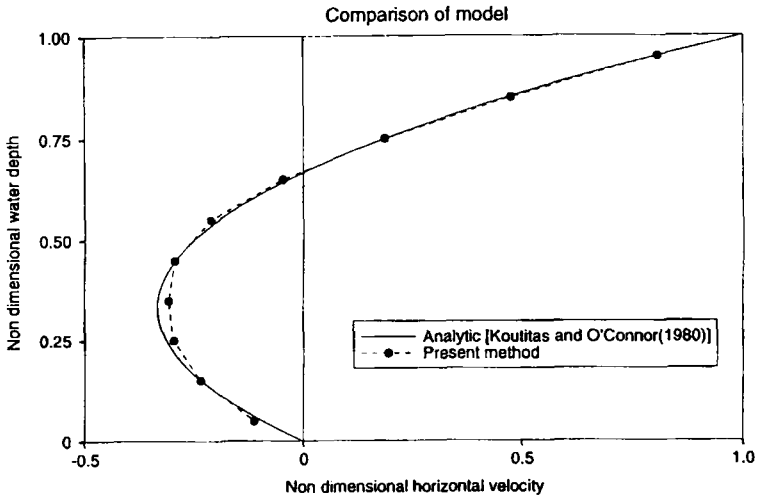

Figure 4. Comparison of theoretical and model velocity profiles

1000 m was used. The simulation assumed that (i) the variable f_m is constant over the depth, (ii) a constant wind-induced shear stress based on a wind velocity of 10 m s^{-1} acts along the free surface and (iii) the water velocity is zero at the channel bottom. Figure 3 shows the computed steady state velocity profile of the wind-driven flow. The theoretical solution[15] is given by the normalized formula

$$u = Z(3Z - 2), \tag{27}$$

where Z is the normalized water depth measured from the channel bottom. Figure 4 shows the normalized velocity profile at a section of the centre of the channel. The result computed by the present method is in good agreement with the theoretical solution.

4. OUTLINE OF TIDAL CURRENT INVESTIGATION OF TOKYO BAY

Since the verification of the multiple-level model is carried out by comparing the numerical results with the observed field data, it is necessary to briefly describe the field measurements here. The measurements of the tidal current in Tokyo Bay were performed during the period from 25 August to 25 October 1983 by the Yokohama Branch, Second Port Construction Bureau, Ministry of Transport, Government of Japan and have been reported in Reference 17.

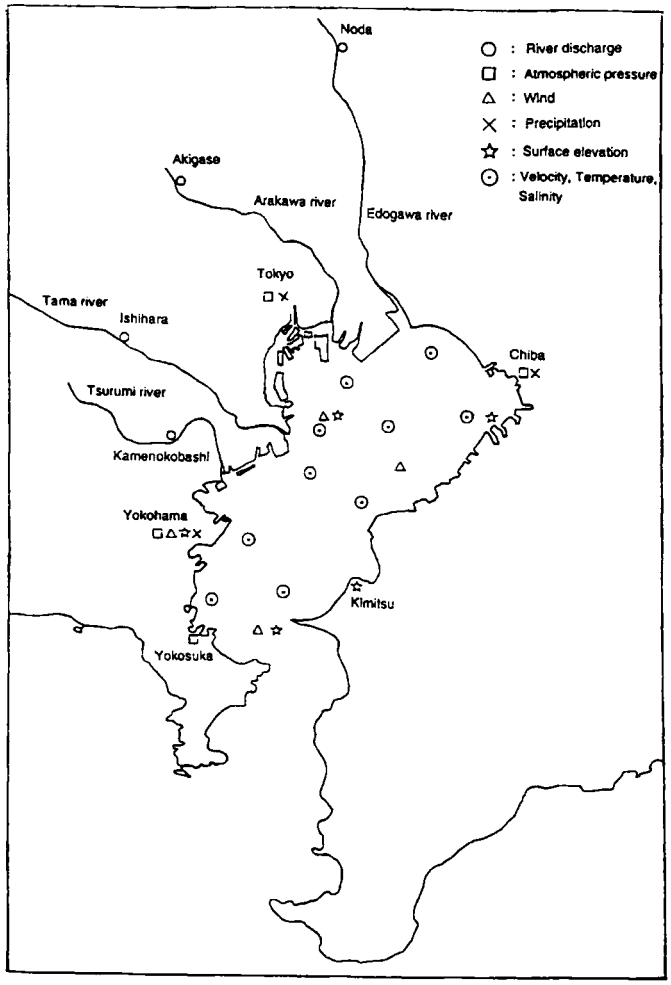

Figure 5. Observation points

The investigation of the tidal current in Tokyo Bay has been carried out to obtain fundamental data on the flow profiles in the Bay. Data such as tide, wind, precipitation, atmospheric pressure, etc. have been taken at the observation points shown in Figure 5 and as indicated in Table I.

Table I. Items of observation

Item	Number of observation points
Velocity	10
Tide	4
Temperature, salinity	10
River discharge	4
Atmosphere pressure	4
Wind	4
Precipitation	3

5. TIDAL CURRENT ANALYSIS OF TOKYO BAY

5.1. Conditions of computations

Finite element idealization. The finite element idealization of Tokyo Bay is shown in Figure 6. The total numbers of nodes and elements at the surface level are 685 and 1216 respectively. The locations where tide gauge records and velocity were measured are also indicated in Figure 6. The constant water depth contours of Tokyo Bay are shown in Figure 7.[18] The flow field is divided into five phases as shown in Figure 8, referring to the bottom configuration of Figure 7.

Physical constants. The physical constants used in the computations are listed in Table II.

Incident wave condition. The constants of the four main tidal constituents are given in Table III.

River inflow discharge. The river discharges considered are given in Table IV.

Interpolation of wind velocity. The steady wind field and the wind speed at each numerical node are linearly interpolated from average values measured at the available wind gauges located around the Bay. Some of these gauges are located quite far from the shore. A maximum wind speed of 10 m s^{-1} was measured in the period of observation of the tidal current.

The hypothetical wind velocity profile is shown in Figure 9.

Calculation of average flow. The velocity of the M_2 constituent at the third cycle, averaged after integrating over one tidal cycle, is adopted as the steady base flow or residual current.

Time increment and selective lumping parameter. The time increment $\Delta t = 15$ s and the selective lumping parameter $e = 0{\cdot}9$ were used in the time integration.

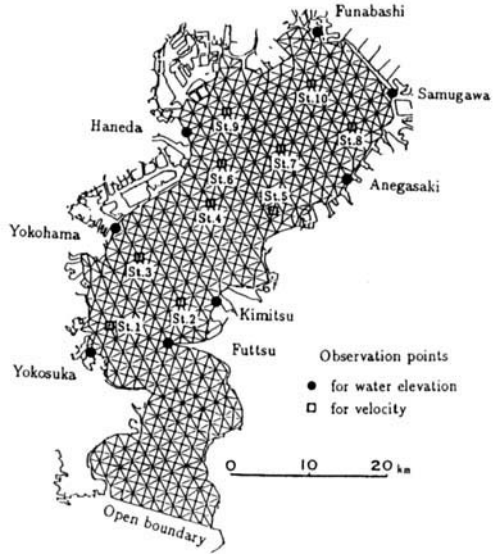

Figure 6. Finite element idealization of Tokyo Bay

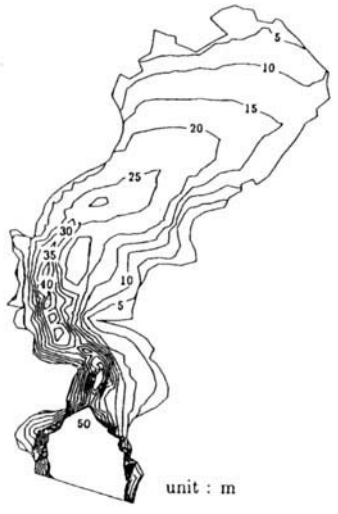

Figure 7. Bottom configuration

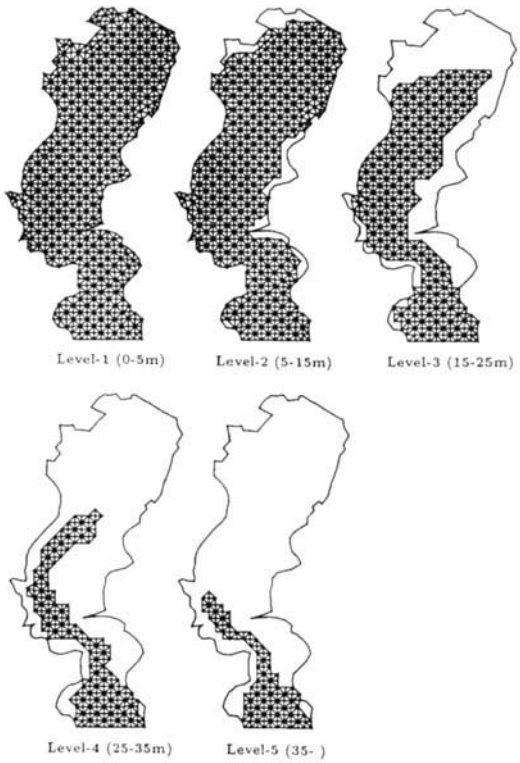

Figure 8. Finite element meshes for each level

Table II. Physical constants

Wind drag coefficient	0·00015
Density of air	$0{\cdot}00129 \times 10^3\,\mathrm{kg\,m^{-3}}$
Friction coefficient at interface	0·001
Friction coefficient at bottom	0·0026
Horizontal eddy viscosity coefficient	$10{\cdot}0\,\mathrm{m^2\,s^{-1}}$
Coriolis parameter	0·000084
Water densities (from surface layer)	$(1{\cdot}010, 1{\cdot}015, 1{\cdot}020, 1{\cdot}025, 1{\cdot}030) \times 10^3\,\mathrm{kg\,m^{-3}}$

Table III. Condition of incident wave

Constituent	Amplitude (m)	Period (h)	Phase delay (rad.)
M_2	0·21	12·42	− 5·8398
S_2	0·15	12·00	− 5·6018
K_1	0·14	23·93	− 1·3290
O_1	0·10	25·82	− 1·3211

Table IV. River inflow discharge

River	Velocity ($m\,s^{-1}$)
Edogawa	1·0
Arakawa	0·5
Tamagawa	0·5
Tsurumigawa	0·5

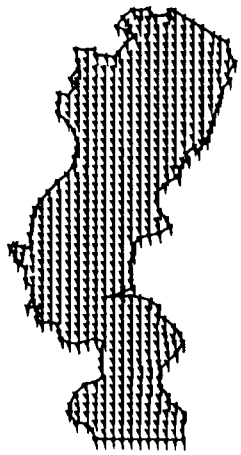

Figure 9. Wind velocity field

5.2. *Steady (time-averaged) flow analysis*

The key effects considered in the test cases are given in Table V.

The computed results of each case were compared with the observed field data for the mean flow. It is seen from Figures 10–15 that the effect of wind shear on the mean flow velocities is much more pronounced than those of the other factors. As expected, the results of Case 6 agree with the field measurements most, because it considered all additional effects. It was also expected that there would be significant discrepancies between the computed flow field and the measured one, because not only is the numerical model still an idealized model with many complicated effects being neglected, but also the field measurements do not have sufficient grid resolution and accuracy. The velocity profile of the whole domain in Case 6 is shown in Figure 16. It is seen that the magnitude of the computed velocities

Table V. Cases of computation

Case	Residual current	Coriolis force	River inflow	Wind stress	Figure
1	Yes	No	No	No	10
2	Yes	Yes	No	No	11
3	Yes	Yes	Yes	No	12
4	No	No	No	Yes	13
5	No	Yes	No	Yes	14
6	No	Yes	Yes	Yes	15, 16

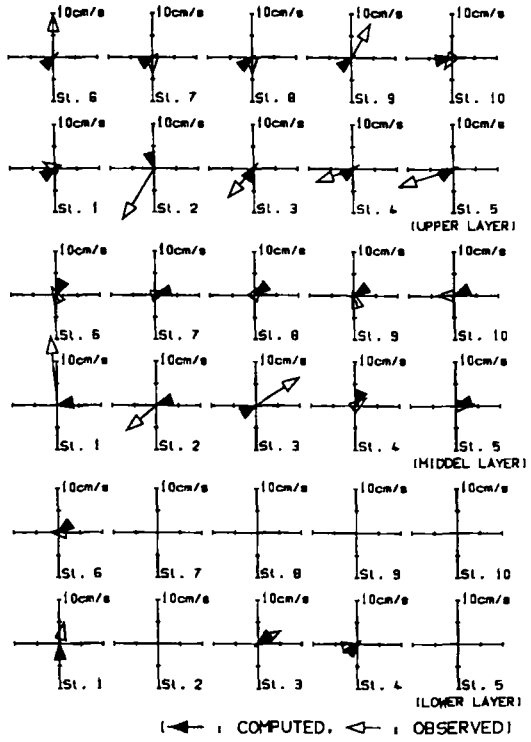

Figure 10. Comparison of velocities (Case 1)

is of the same order as the observed values, but the values for surface velocity are relatively larger than those of the observations.

The contributions of each factor were evaluated by comparing the kinetic energy computed in each case with that from Case 6. The summation of kinetic energy at 24 observation points was defined by

$$E = \tfrac{1}{2} \sum_{i=1}^{24} u_i^2,$$

where u_i is the absolute value of velocity at the ith observation point. The kinetic energy of Case 6 is assumed to be 100%. The contributions of each factor were defined as

$$E_{\text{wind effect}} = \frac{E_{\text{Case 6}} - E_{\text{Case 3}}}{E_{\text{Case 6}}} \times 100 = 90{\cdot}54\%,$$

$$E_{\text{river effect}} = \frac{E_{\text{Case 3}} - E_{\text{Case 2}}}{E_{\text{Case 6}}} \times 100 = 9{\cdot}34\%,$$

$$E_{\text{Coriolis effect}} = \frac{E_{\text{Case 2}} - E_{\text{Case 1}}}{E_{\text{Case 6}}} \times 100 = 0{\cdot}12\%,$$

where $E_{\text{Case 1}} = 0{\cdot}00026$, $E_{\text{Case 2}} = 0{\cdot}00013$, $E_{\text{Case 3}} = 0{\cdot}01038$ and $E_{\text{Case 6}} = 0{\cdot}10969$ m^2 s^{-2}. From these comparative studies it may be concluded again that the wind effect is the most important factor among the three considered in this study in simulating the mean (base) flow in Tokyo Bay. However, the Coriolis term should not be neglected in the mean flow analysis even though its contribution is small.

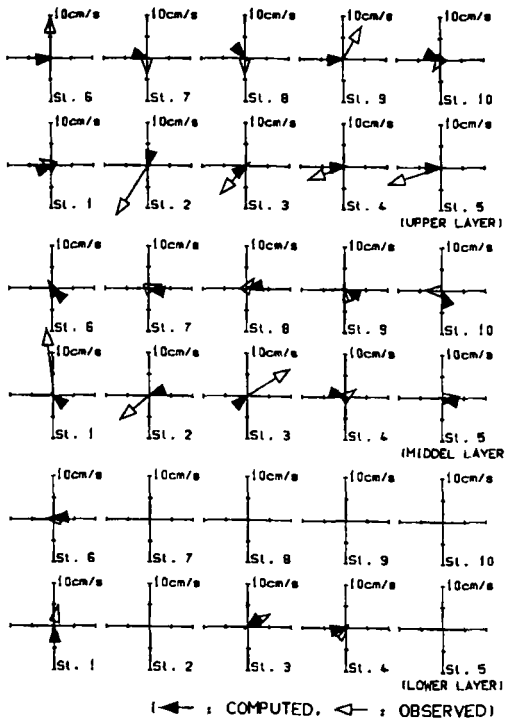

Figure 11. Comparison of velocities (Case 2)

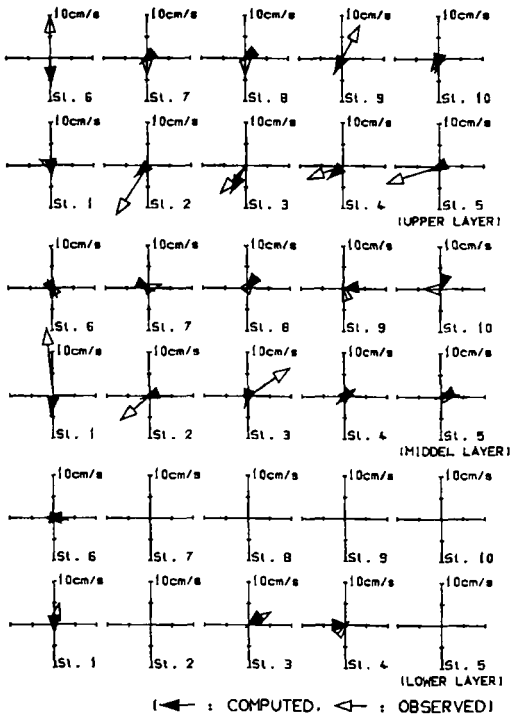

Figure 12. Comparison of velocities (Case 3)

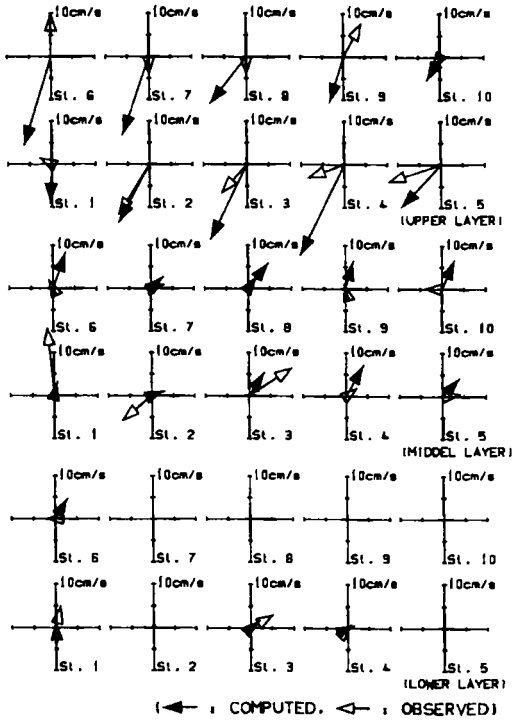

Figure 13. Comparison of velocities (Case 4)

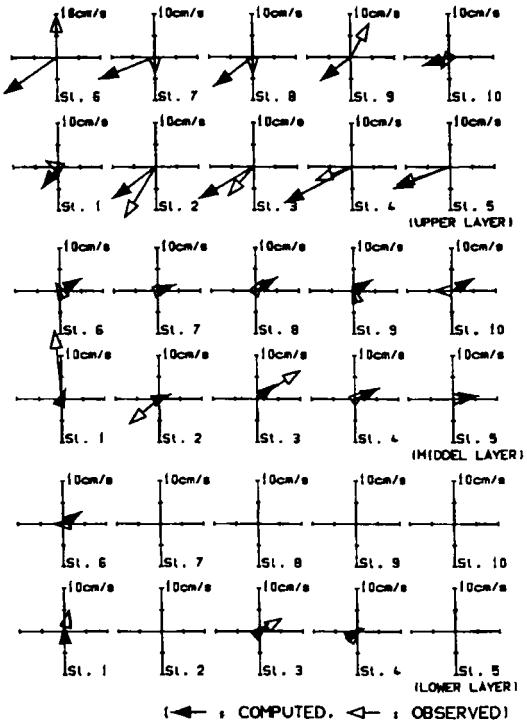

Figure 14. Comparison of velocities (Case 5)

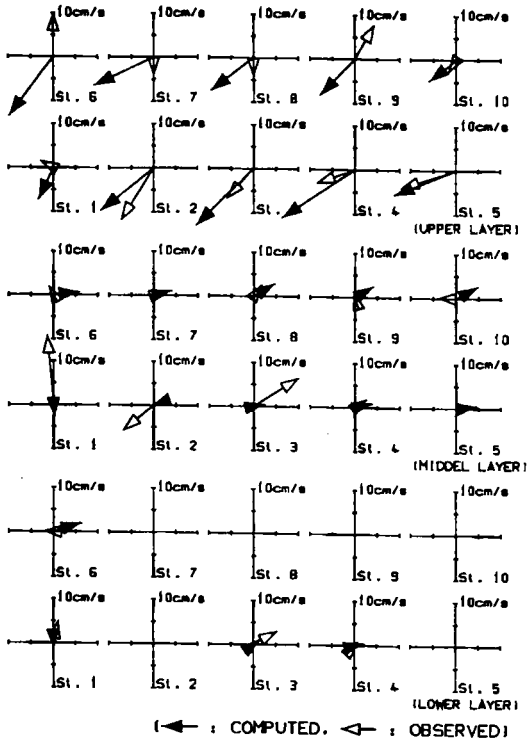

Figure 15. Comparison of velocities (Case 6)

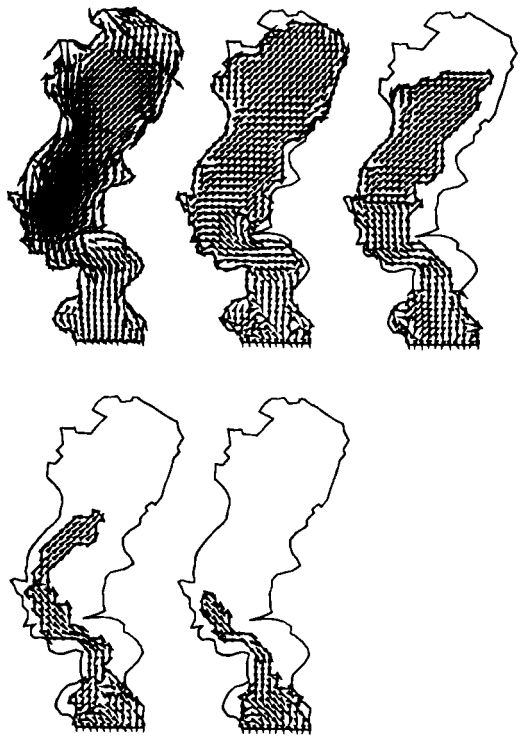

Figure 16. Computed velocity field (Case 6)

5.3. Tidal current analysis with M_2 constituent

The M_2 constituent, which has a period of 12·42 h, is imposed on the open boundary as

$$\bar{\eta}^{\mathrm{I}} = a_{\mathrm{I}} \sin\left(\frac{2\pi}{T} t\right),$$

where $a_I = 0{\cdot}25$ m was estimated by the parametric identification method.[19] Two computations with and without the Coriolis term were carried out. The results of tidal velocity were compared with those measured at gauging stations for the surface, middle and lower levels and are shown graphically as ellipses in Figures 17 and 18.

It is seen that these results agree well with the observed data. The velocity trajectories of the case with the Coriolis term are closer to the observed ellipses than those of the case without the Coriolis force. At a few stations the direction of the present tidal current velocity does not match with the observed data for both cases tested; however, the magnitudes show good agreement. This might be caused by errors in measurement or observation point positioning.

5.4. Tidal current analysis with four main constituents

The four main constituents of the tide are imposed as

$$\bar{\eta}^{\mathrm{I}} \sum_{m=1}^{4} a_m \sin\left(\frac{2\pi}{T_m} t - \kappa_m\right),$$

where the constants are as listed in Table III. The amplitudes of the constituents were estimated by the parametric identification method.[19] The three cases studied are specified in Table VI.

The time variation of the surface elevation under the conditions of Case 1 is compared in Figure 19 with the observed tidal levels. The computed surface elevations are seen to be in good agreement with the observed ones. Similar results were obtained in the other cases tested.

The computed velocities and measured data for the maximum north-west and south-east streams are compared in Figures 20–22 for each of the cases. In Cases 1 and 2 the computed velocities are good in agreement with the measured velocities at the surface, middle and lower levels. However, discrepancies are observed in Case 3, which could be caused by the fact that the Coriolis force term was neglected.

6. CONCLUDING REMARKS

The main conclusions obtained are as follows.

1. An improved multiple-level model with a new open boundary condition treatment was developed. The results of wind shear effect on the free surface flow in a rectangular basin as predicted by the improved multiple-level model are in excellent agreement with those obtained by Koutitas and O'Connor.[15] This evidence clearly verifies that the mathematical formulation, numerical solution techniques, computational algorithm, boundary/initial conditions and

Table VI. Cases of computation

Case	Coriolis term	River inflow	Wind stress	Figure
1	Yes	Yes	Yes	19, 20
2	Yes	No	No	21
3	No	Yes	Yes	22

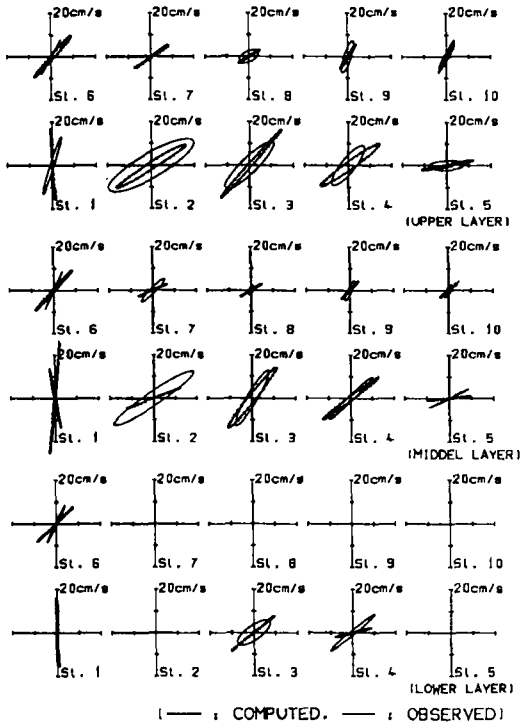

Figure 17. Comparison of tidal ellipses with Coriolis force

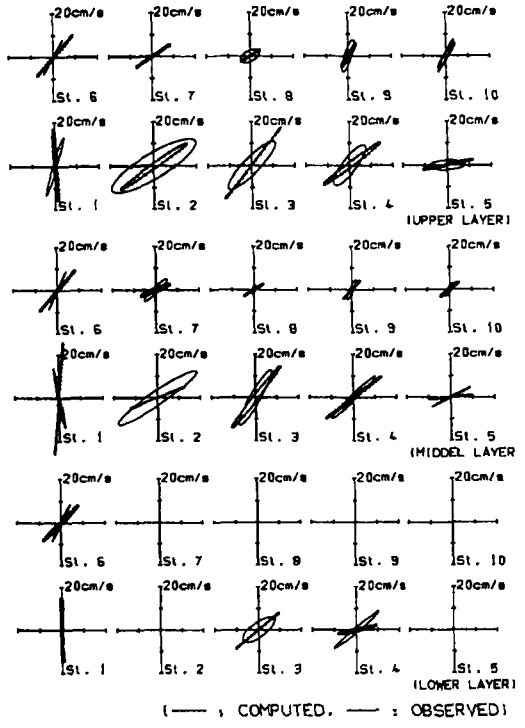

Figure 18. Comparison of tidal ellipses without Coriolis force

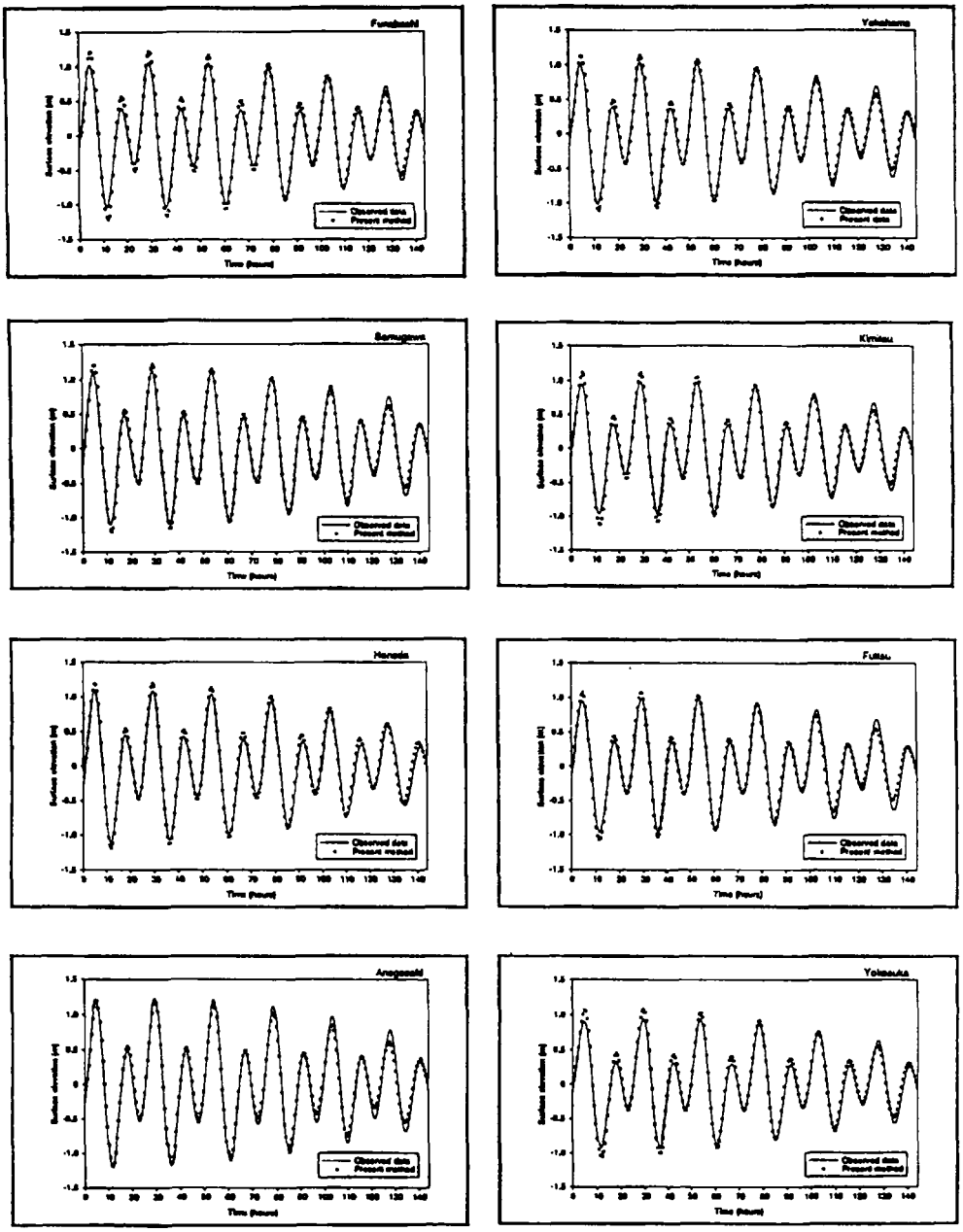

Figure 19. Time variation of surface elevation (Case 1)

physical/numerical parameters selected are correct. This is the first step of the two-step numerical model verification process adopted by the ASCE Task Committee on 3D Free Surface Hydrodynamic Model Verification.

2. With the inclusion of Coriolis force, river inflow and wind shear effects in the multiple-level model, more realistic flow fields have been simulated. This study represents a significant improvement in modelling coastal flows and transport phenomena. However, one must not forget

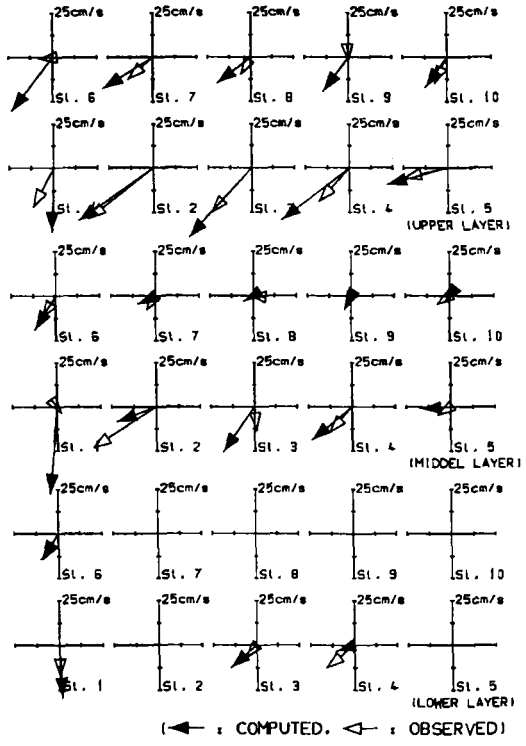

Figure 20(a). Computed velocities and observed data (Case 1, downstream)

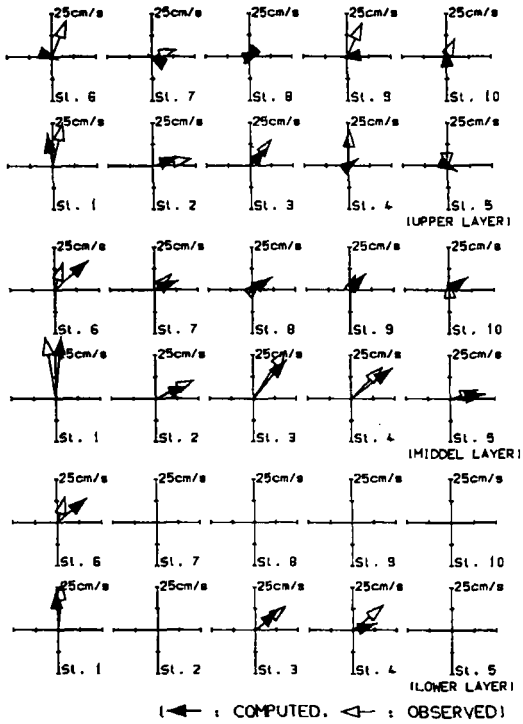

Figure 20(b). Computed velocities and observed data (Case 1, upstream)

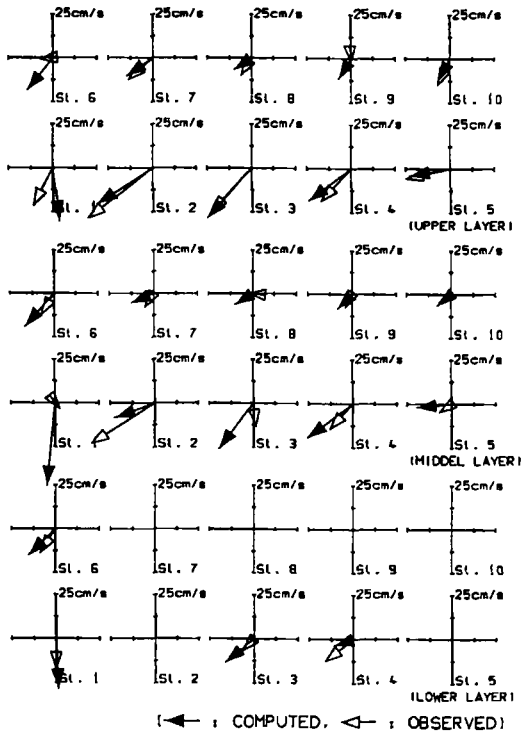

Figure 21(a). Computed velocities and observed data (Case 2, downstream)

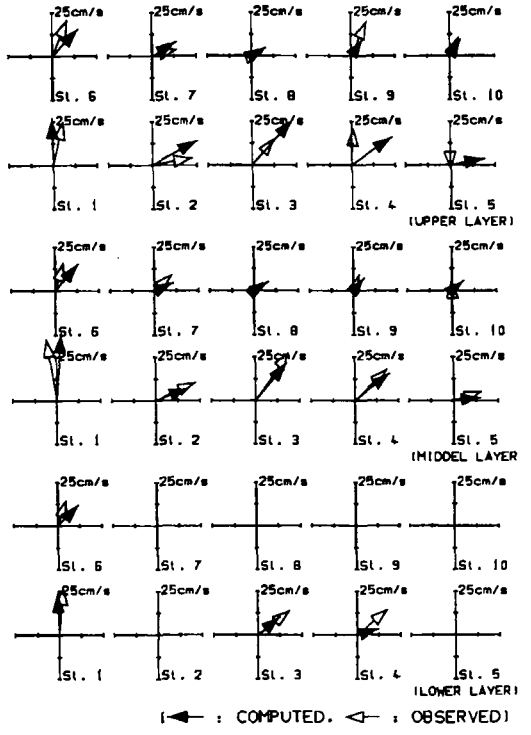

Figure 21(b). Computed velocities and observed data (Case 2, upstream)

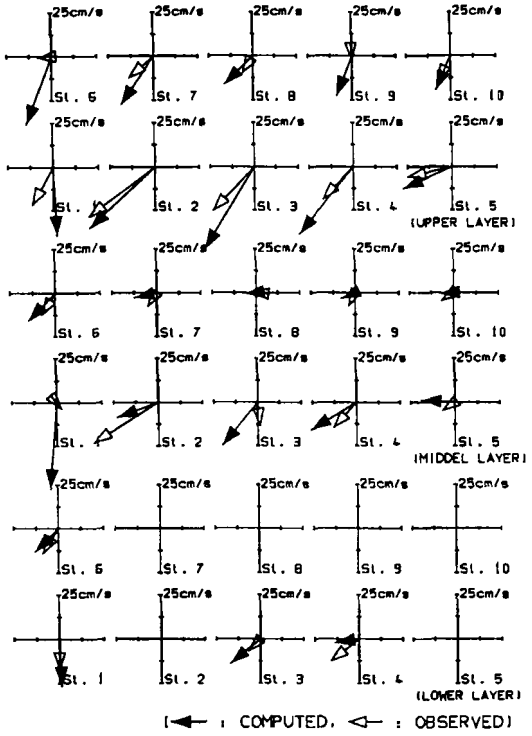

Figure 22(a). Computed velocities and observed data (Case 3, downstream)

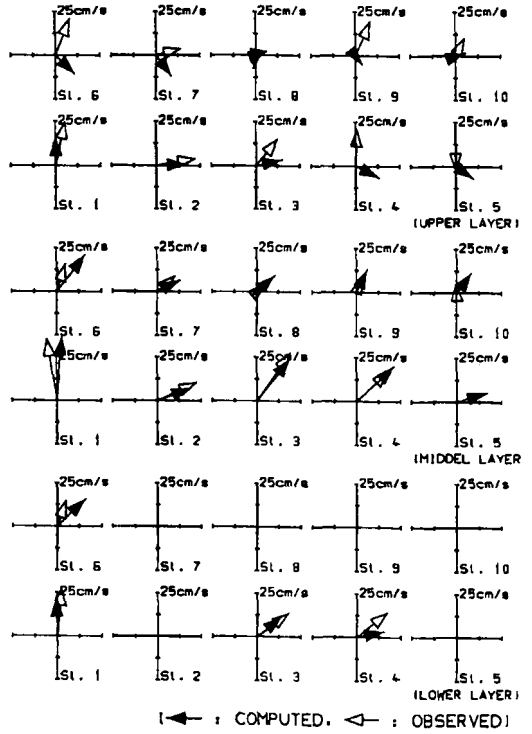

Figure 22(b). Computed velocities and observed data (Case 3, upstream)

that additional studies are needed to simulate realistic coastal flows, because there are still quite a number of complicated physical processes which have not or could not be considered here.

3. The implementation of a newly developed treatment of the open boundary condition in simulating coastal flows has improved the quality of numerical solutions by eliminating or reducing some spurious artificial waves. As a result, the accuracy and stability of the numerical model have been enhanced.
4. A mean or base flow analysis in Tokyo Bay was carried out and the results have been compared with those measured. The results show that the wind effect is one of the most important forcing factors in producing realistic simulations in Tokyo Bay. Although the effect of the Coriolis term is not as important, it should not be neglected in the mean flow simulation of real world problems especially in predicting transport phenomena.
5. Tidal current analyses with the M_2 constituent and the four main constituents in Tokyo Bay were carried out. Comparison of the tidal ellipses between the computed and observed results shows that the Coriolis term is an important factor in accurately predicting the periodic flow field. From comparisons of the simulated tidal velocities with the observed data in the case of considering the four main constituents, it is not surprising to find that the most realistic prediction is obtained for the case which includes all forcing effects, i.e. tides, Coriolis force, wind shear stress and river inflow. The reasonable agreement between the computational simulation of tidal and residual currents of Tokyo Bay and the measured field data completes the second step of the two-step computational model verification process adopted by the ASCE Task Committee. Therefore the improved multiple-level model has been validated as a research tool for studying flow and transport phenomena in coastal waters.

REFERENCES

1. H. P. Wang, 'Multi-level finite element hydrodynamical model of Block Island Sound', in G. Pinder *et al.* (eds), *Finite Element in Water Resources*, Pentech, 1975, pp. 4-69–4-93.
2. M. Kobayashi, K. Nakata and M. Kawahara, 'A three-dimensional multi-leveled finite element method for density current analysis', in R. H. Gallagher *et al.* (eds), *Finite Element Method in Flow Problems, II*, 1980, pp. 80–92.
3. M. Kawahara, M. Kobayashi and K. Nakata, 'Multiple level finite element analysis and its applications to tidal current flow in Tokyo Bay', *Appl. Math. Model.*, **7**, 197–211 (1983).
4. R. W. Lardner and H. M. Cekirge, 'A new algorithm for three-dimensional tidal and storm surge computation', *Appl. Math. Model.*, **12**, 471–481 (1988).
5. D. R. Lynch and F. E. Werner, 'Three-dimensional hydrodynamics on finite element. Part II: Non-linear time-stepping', *Int. j. numer. methods fluids*, **12**, 507–533 (1991).
6. T. Kodama and M. Kawahara, 'Multiple level finite element analysis for tidal current flow with non-reflective open boundary condition', *Proc. JSCE*, **446(I-19)**, 77s–87s (1992).
7. S. S. Y. Wang and K. K. Hu, 'Improved methodology for formulating finite element hydrodynamic models', in T. J. Cheung (ed.), *Finite Element in Fluids*, Vol. 8, Hemisphere, New York, 1992, pp. 457–478.
8. X. Jin and C. Kranenburg, 'Quasi-3D numerical modeling of shallow-water circulation', *J. Hydraul., ASCE*, **119**, 458–471 (1993).
9. M. Kawahara, H. Hirano, K. Tsubota and K. Inagaki, 'Selective lumping finite element method for shallow water flow', *Int. j. numer. methods fluids*, **2**, 89–112 (1982).
10. H. Liu and H. J. Perez, 'Wind-induced circulation in shallow water', *J. Hydraul. Div., ASCE*, **97**, 923–935 (1971).
11. R. H. Gallagher and S. T. K. Chan, 'Higher-order finite element analysis of lake circulation', *Comput. Fluids*, **1**, 119–132 (1973).
12. R. H. Gallagher, J. A. Liggett and S. T. K. Chan, 'Finite element shallow lake circulation analysis', *J. Hydraul. Div., ASCE*, **99**, 1083–1096 (1973).
13. B. M. Jamart and J. Ozer, 'Comparison of 2-D and 3-D models of the steady wind-driven circulation in shallow waters', *Coastal Eng.*, **11**, 393–413 (1987).
14. I. K. Tsanis, 'Simulation of wind-induced water currents', *J. Hydraul. Eng., ASCE*, **115**, 1113–1134 (1989).
15. C. Koutitas and B. O'Connor, 'Modeling three-dimensional wind-induced flows', *J. Hydraul. Div., ASCE*, **106**, 1843–1865 (1980)
16. B. R. Pearce and C. K. Cooper, 'Numerical circulation model for wind induced flow', *J. Hydraul. Div., ASCE*, **107**, 285–302 (1981).

17. Yokohama Branch, Second Port Construction Bureau, Ministry of Transport, Government of Japan, *Report of Measurements of Tidal Current in Tokyo Bay*, 1983, (in Japanese).
18. Maritime Safety Agency, *Maritime Chart of Tokyo Datum*, 1984, p. 90.
19. T. Kodama, T. Kawasaki and M. Kawahara, 'A finite element method for shallow water equation including open boundary condition', *Int. j. numer. methods fluids*, **13**, 939–953 (1991).
20. Maritime Safety Agency, *Harmonic Constant Table*, 1989.